Research Square

Preprints are preliminary reports that have not undergone peer review.
They should not be considered conclusive, used to inform clinical practice,
or referenced by the media as validated information.

The DIAS: quantifying coupled curve intersections in pharmacology, ecology, demography, and climatology

Rafael Dias de Brito Oliveira

rdbo@fisio.grad.ufmg.br

Universidade Federal de Minas Gerais https://orcid.org/0000-0001-9663-905X

Method Article

Keywords: Applied statistics, Coupled curves, Delta method, Intersection point, Parametric bootstrap

Posted Date: October 30th, 2026

DOI: https://doi.org/10.21203/rs.3.rs-11484088/v1

License: This work is licensed under a Creative Commons Attribution 4.0 International License.
Read Full License

Additional Declarations: The authors declare no competing interests.

The DIAS: quantifying coupled curve intersections in pharmacology, ecology, demography, and climatology

Author: Rafael Dias de Brito Oliveira

Ph.D. candidate in Physiology and Pharmacology. Institute of Biological Sciences, Universidade Federal de Minas Gerais (UFMG), Belo Horizonte - MG, Brazil.

E-mail: rdiasdbo@gmail.com | ORCID: 0000-0001-9663-905X

ABSTRACT:

The comparison of coupled curves arises in many applied sciences. In vascular physiology, researchers ask how mediator production and vascular relaxation intersect as the concentration of a signalling molecule changes. In ecology, they ask when predator consumption and prey survival are balanced. In demography, they ask when the urban population surpasses the rural population. In all these cases, the point of intersection between two curves is often assessed visually, without formal uncertainty quantification. The Dias' Intercept Analysis System (DIAS) is a practical framework for estimating the intersection point of two coupled curves and for comparing that point. The DIAS treats the intersection as a bivariate random vector, propagates uncertainty via the Delta Method, and provides a calibrated comparison through a parametric bootstrap procedure. Monte Carlo simulations show that the DIAS estimator is approximately unbiased and that its confidence intervals achieve coverage close to the nominal level. The method is illustrated through applications in pharmacology, ecology, demography, and climatology. In each case, the DIAS provides an estimate of the intersection point with interpretable uncertainty, allowing comparisons that would be difficult to make reliably by visual inspection alone. A free, open-source Shiny application makes it accessible to researchers without programming expertise.

KEYWORDS: Applied statistics; Coupled curves; Delta method; Intersection point; Parametric bootstrap.

1. INTRODUCTION

In the study of complex biological, ecological, and physical systems, researchers frequently encounter paired variables whose relationship is described by coupled curves: two functions that share the same independent variable and whose responses evolve in tandem. This pattern appears across numerous academic fields, including the production of a signalling mediator and the resulting physiological effect in pharmacology [1], the cumulative consumption of prey and the survival of the predator in ecology [2], the urban and rural fractions of a population over time in demography, and the expression of circadian clock genes throughout the day in biology [3, 4]. In each case, we can ask: where do these curves intersect, and does that intersection point differ meaningfully between experimental groups or observational periods?

Despite the broad relevance of this problem, the statistical toolkit available to researchers remains surprisingly limited. The dominant approach is visual inspection: an investigator overlays two fitted curves, notes where they cross, and judges whether the crossing point appears to shift between conditions. This practice, while intuitive, lacks formal inference, and it provides no estimate of uncertainty for the intersection coordinates, no confidence interval, and no hypothesis test. More sophisticated analyses typically reduce the problem to comparing individual curve parameters. In pharmacology, for instance, one may compare the EC50 values of two dose-response curves [4]; in survival analysis, one may test whether two Kaplan-Meier curves are globally different using the log-rank test, even when the curves cross and the proportional hazards assumption is violated [5]. These approaches, although statistically rigorous, address a different question: they compare summary parameters or whole curves, not the point of intersection itself.

The methodological gap becomes particularly evident when surveying the literature on curve comparison. Herberich et al. (2014) [6] developed a framework for multiple comparisons of nonlinear curves using penalised splines and simultaneous inference, capable of identifying specific positions along the x-axis where two curves differ. Oleson et al. (2017) [7] proposed a bootstrap-based procedure to detect time-specific differences between temporal nonlinear curves while controlling the family-wise error rate. Hristova and Wimley (2023) [8] described a spreadsheet-implementable method that yields a global p-value for the difference between two arbitrary curves. These contributions,

among others [9, 10], share a common limitation: they test whether curves differ, but they do not estimate the point at which they are equal.

The absence of a dedicated method for the intersection point contrasts with the availability of two well-established statistical techniques that, when combined, provide a natural solution. The first is the Delta Method [11], which allows the propagation of uncertainty from estimated model parameters to any derived quantity. The Delta Method is routinely used to compute standard errors and confidence intervals for nonlinear functions of parameters, such as the area under a curve, the maximum of a function, or the EC50 of a single sigmoid. An accessible review of its applications in modern statistics is provided in the WIREs Computational Statistics article [12]. The second technique is the bivariate Wald test (also known as Hotelling's T^2 test when covariance matrices are estimated), which provides a formal hypothesis test for the equality of two-dimensional vectors. The Wald test has a long history in econometrics [13] and continues to be widely applied in fields ranging from fisheries science [14] to modern high-dimensional inference [15, 16]. Practical implementations are described in recent tutorials [17].

In this paper, we propose the Dias' Intercept Analysis System (DIAS), a method for estimating and comparing the intersection point of two coupled curves. The DIAS treats the intersection as a bivariate random vector, propagates its uncertainty via the Delta Method, and enables formal comparisons between groups using the Wald test. In the framework, when multiple intersections exist, the method applies separate comparisons to each pair of corresponding DIAS points, with a multiplicity adjustment (e.g., Bonferroni) to control the family-wise error rate. The approach is model-independent, requiring only that the two curves can be fitted and that their intersection can be computed numerically. Crucially, the DIAS does not require the assumption of a single, existing intersection: it allows for the numerical search of intersections within a specified interval, and when multiple intersections exist, it provides formal comparisons for each pair with appropriate multiplicity control.

2. METHODS

2.1. The Dias' Intercept Analysis System (DIAS)

Consider two coupled curves, $f_1(x|\theta_1)$ and $f_2(x|\theta_2)$, where $\theta_1 \in \mathbb{R}^{p1}$ and $\theta_2 \in \mathbb{R}^{p2}$ are vectors of parameters to be estimated from data. The curves are coupled in the

sense that they share the same predictor x and their responses are measured on comparable scales, e.g., two dose–response curves, two time series, or two complementary percentages.

The raw intersection point (x^*, y^*) is defined implicitly by the system

$$\begin{cases} f_1(x^* \mid \theta_1) = y^*, \\ f_2(x^* \mid \theta_2) = y^*. \end{cases} \tag{1}$$

Because θ_1 and θ_2 are estimated from finite samples, (x^*, y^*) is a random vector. The DIAS is the full inferential object that comprises:

- The point estimate ($\hat{x}^*$, $\hat{y}^*$) obtained by plugging the estimated parameters $\hat{\theta} = (\hat{\theta}_1, \hat{\theta}_2)$ into the system above.
- The uncertainty of this estimate, quantified by a 2 × 2 covariance matrix Σ_{DIAS}.

The DIAS transforms the problem of "where do these curves meet?" into a formal statistical estimation problem with a bivariate outcome.

2.2. Error propagation via the Delta Method

Let $\hat{\theta} = (\hat{\theta}_1{}^T, \hat{\theta}_2{}^T)^T$ be the combined $p \times 1$ parameter vector, where $p = p_1 + p_2$. Under standard regularity conditions for maximum likelihood or least-squares estimation, $\hat{\theta}$ is asymptotically normal with mean θ and covariance matrix $\Sigma_{\hat{\theta}}$. Because the two curves are fitted to independent data, $\Sigma_{\hat{\theta}}$ is block-diagonal:

$$\Sigma_{\hat{\theta}} = \begin{pmatrix} \Sigma_{\hat{\theta}_1} & 0_{p_1 \times p_2} \\ 0_{p_2 \times p_1} & \Sigma_{\hat{\theta}_2} \end{pmatrix}, \tag{2}$$

where $\Sigma_{\hat{\theta}_i}$ is the covariance matrix of the estimator $\hat{\theta}_i$. For nonlinear models fitted by least squares, $\Sigma_{\hat{\theta}_i} \approx \hat{\sigma}_i^2 (J_i{}^T J_i)^{-1}$, with J_i being the Jacobian of the model function with respect to its parameters and $\hat{\sigma}_i^2$ the residual variance. More generally, for maximum likelihood, $\Sigma_{\hat{\theta}_i}$ is the inverse of the Fisher information matrix.

Define the function $g: \mathbb{R}^p \to \mathbb{R}^2$ that maps the full parameter vector to the intersection point:

(3)

$$g(\theta) = \begin{pmatrix} x^*(\theta) \\ y^*(\theta) \end{pmatrix}.$$

The Delta Method provides an approximation to the covariance matrix of $g(\hat{\theta})$:

$$\Sigma_{DIAS} = J\Sigma_{\hat{\theta}} J^T, \tag{4}$$

where J is the $2 \times p$ Jacobian matrix of g evaluated at $\hat{\theta}$:

$$J = \begin{pmatrix} \frac{\partial x^*}{\partial \theta_1} & \cdots & \frac{\partial x^*}{\partial \theta_p} \\ \frac{\partial y^*}{\partial \theta_1} & \cdots & \frac{\partial y^*}{\partial \theta_p} \end{pmatrix}. \tag{5}$$

Except for very simple models, x^* and y^* do not have closed-form expressions in terms of θ. We therefore approximate the partial derivatives numerically using central finite differences with a step size $h = 10^{-6}$:

$$\frac{\partial g_k}{\partial \theta_j} \approx \frac{g_k(\hat{\theta} + he_j) - g_k(\hat{\theta} - he_j)}{2h}, \tag{6}$$

where e_j is the $j-th$ unit vector. This numerical approach is fully general and applies to any pair of curves for which the intersection can be computed.

The choice of the finite-difference step $h = 10^{-6}$ was assessed by recomputing the DIAS with step sizes ranging from $h = 10^{-4}$ to $h = 10^{-8}$. The resulting estimates and standard errors were essentially unchanged, indicating that the numerical approximation is stable under these conditions. Details are provided in the Supplementary Material.

From Σ_{DIAS} we obtain the standard errors

(7)

$$SE(\hat{x}^*) = \sqrt{(\Sigma_{DIAS})_{11}} \quad | \quad SE(\hat{y}^*) = \sqrt{(\Sigma_{DIAS})_{22}}$$

and the covariance between $\hat{x}^*$ and $\hat{y}^*$, which is essential because the two coordinates are usually correlated.

2.3. Comparing DIAS values between groups

When two independent groups (e.g., control and treatment) are available, the DIAS can be computed separately for each group and compared. Two procedures are offered in the present implementation: a bivariate Wald test and a parametric bootstrap test. The bivariate Wald test is defined as follows. Let $\Delta = (\hat{x}_1^* - \hat{x}_2^*, \hat{y}_1^* - \hat{y}_2^*)^T$ be the difference between the two estimated DIAS vectors, and let $\Sigma 1$ and $\Sigma 2$ be the corresponding covariance matrices. The Wald statistic is

$$W = \Delta^T(\Sigma_1 + \Sigma_2)^{-1}\Delta. \tag{8}$$

Under standard regularity conditions and for sufficiently large samples, W follows approximately a chi-squared distribution with two degrees of freedom. The effect size is summarised by the Mahalanobis distance $D = \sqrt{W}$. Although the Wald test is quick and convenient, our simulations indicated that it can be liberal for small samples and nonlinear models. We therefore also implemented a parametric bootstrap procedure.

In the parametric bootstrap, the two groups are assumed to share the same underlying curves under the null hypothesis. The fitted models from the two groups are pooled to obtain common parameter estimates. New datasets are then simulated from these pooled models, the DIAS is recomputed for each pair of simulated groups, and the observed W statistic is compared with the empirical distribution of simulated W values. The bootstrap p-value is the proportion of simulated W values greater than or equal to the observed W.

We recommend the bootstrap p-value for confirmatory conclusions, especially when the sample size is small or the model is nonlinear. The Wald test is retained in the application as a fast exploratory tool. When each group exhibits multiple intersections (e.g., periodic curves), the same comparison procedures can be applied separately to

each pair of corresponding DIAS points. To control the family-wise error rate across multiple comparisons, p-values may be adjusted using Bonferroni, Holm, or similar corrections.

2.4. Confidence ellipses

The bivariate normal approximation for ($\hat{x}^*, \hat{y}^*$) allows the construction of confidence regions. A 100(1 − α)% confidence ellipse for a single DIAS is the set

$$\{v \in \mathbb{R}^2 : (v - \hat{v})^T \Sigma_{DIAS}^{-1} (v - \hat{v}) \leq x_{2,1-\alpha}^2\}, \quad (9)$$

were $\hat{v} = (\hat{x}^*, \hat{y}^*)^T$. The ellipse is centered at $\hat{v}$, and its shape reflects the covariance structure: a narrow ellipse indicates high precision, a strong tilt indicates correlation between $\hat{x}^*$ and $\hat{y}^*$. Plotting the ellipses for two groups on the same axes provides an intuitive visual comparison: non-overlapping ellipses suggest a clear difference, but the formal comparison should be performed with the methods described in the previous section.

2.5. Simulation validation

To evaluate the finite-sample performance of the DIAS estimator, we conducted a Monte Carlo simulation study covering the linear, sigmoid, and cosine models under a range of sample sizes and noise levels. The results suggest that the DIAS is approximately unbiased, that its standard errors yield confidence intervals with coverage close to the nominal 95% level for moderate sample sizes, and that the cosine model requires slightly larger samples to achieve the same precision, which is a finding consistent with the difficulty of estimating phase in periodic curves. These simulations support the validity of the Delta Method approximation for the DIAS. In addition, the parametric bootstrap was evaluated for type I error and power for linear and sigmoid models; the results are reported in the Supplementary Material. The bootstrap controlled the Type I error rate close to the nominal level and achieved high power for moderate-to-strong effects under low-to-moderate noise.

2.6. Software implementation

The DIAS method has been implemented as a free, open-source Shiny web application to facilitate its use by researchers without programming expertise. The

app allows the user to upload data, select a model form (e.g., linear, sigmoid, cosine), and automatically compute the DIAS, standard errors, Wald tests, parametric bootstrap p-values, and confidence ellipses. The specific functional forms supported are described in the Supplementary Material. The app code is available at [https://r-dias.shinyapps.io/DIAS/].

2.7. Graphical representations

All curve fittings and graphical reconstructions of the results section were performed using GraphPad Prism (version 10.2.3; GraphPad Software, San Diego, CA). For the reanalysis of published data, raw data points were extracted from the original figures using WebPlotDigitizer (Rohatgi, 2022), a validated tool for recovering numerical data from graphical representations. The extracted coordinates were then imported into Prism, where the original dose–response or time-course curves were reconstructed as appropriate. For the original data applications, raw data were obtained directly from the Brazilian Institute of Geography and Statistics (IBGE) and the Brazilian National Institute of Meteorology (INMET), respectively. All DIAS calculations, error propagation via the Delta Method, Wald tests, and parametric bootstrap comparisons were performed using the DIAS Shiny application.

3. SIMULATIONS

3.1. Design

To evaluate the finite-sample properties of the DIAS estimator and the coverage of its confidence intervals, we conducted a Monte Carlo simulation study covering three representative models: linear, 3-parameter sigmoid, and cosine.

For each model, we defined a set of *true* parameter values that produce a known intersection point (**Table 1**). Data were generated by adding independent Gaussian noise $N(0, \sigma^2)$ to the true curves, with three noise levels ($\sigma = 1, 2, 5$) and three sample sizes ($n = 6, 10, 20$ equally spaced points). These choices span the range from small, noisy experiments (typical in pharmacology) to larger, more precise observational studies (typical in demography or climatology).

For each of the $3 \times 3 \times 3 = 27$ scenarios (model $\times n \times \sigma$), we generated $N = 1{,}000$ independent datasets. On each dataset, we fitted the two curves by least squares (linear regression for the linear model, nonlinear least squares via the Levenberg-

Marquardt algorithm for the sigmoid and cosine models) and computed the DIAS using the Delta Method as described in Section 2.2. Replicates in which the model fitting failed to converge were excluded from the summary statistics; convergence rates are reported alongside the results. For each scenario, we recorded:

- Bias: the difference between the mean estimated DIAS and the true value.
- Root mean squared error (RMSE): $\sqrt{\frac{1}{N}\sum(\hat{x}^* - x^*)^2}$ (analogous for y).
- Empirical coverage of the 95% confidence interval: the proportion of replicates in which the true value lay within the interval $\hat{x}^* \pm 1.96 \times \mathrm{SE}(\hat{x}^*)$.

Table 1. True parameters for DIAS.

Model	Parameters (Curve 1)	Parameters (Curve 2)	True DIAS (x^*, y^*)
Linear	$a_1 = 0$, $b_1 = 1$	$a_2 = 10$, $b_2 = -1$	(5,5)
Sigmoide 3P	$\mathrm{Top}_1 = 100$,	$\mathrm{Top}_2 = 80$,	(−7.45,26.0)
	$\mathrm{Bottom}_1 = 0$,	$\mathrm{Bottom}_2 = 20$,	
	$\mathrm{LogEC50}_1 = -7$	$\mathrm{LogEC50}_2 = -6.5$	
Cosine	$\mathrm{Mesor}_1 = 20$,	$\mathrm{Mesor}_2 = 25$,	(0.29,23.1)†
	$\mathrm{Amp}_1 = 5$,	$\mathrm{Amp}_2 = 3$,	
	$\mathrm{Phase}_1 = 2$	$\mathrm{Phase}_2 = 8$	

† First of two intersections per period; the second occurs at $x \approx 9.5$.

3.2. Results

Table 2 summarises the simulation results for the linear model. The bias of the DIAS was negligible across all linear-model scenarios (<0.11 in absolute value for x^*, <0.11 for y^*). The RMSE decreased systematically with increasing sample size and increased with noise level, as expected. Coverage of the confidence intervals remained close to the nominal 95% for both coordinates in most scenarios. A modest under-coverage was observed for x^* at the smallest sample size (91-96%), which is consistent with the asymptotic nature of the Delta Method; coverage improved to 93-97% for $n = 10$ and 20.

Results for the 3-parameter sigmoid model are presented in **Table 3**. The DIAS again exhibited small bias (<0.02 for x^*) and low RMSE (e.g., 0.028 for $n = 6$, $\sigma = 1$). Coverage for x^* ranged from 89% to 96%, while coverage for y^* was slightly lower (82-90%), reflecting the greater uncertainty in estimating the vertical position of the intersection when the curves are nonlinear. Convergence rates exceeded 99% in all scenarios.

The cosine model, which yields two intersections per cycle, proved the most challenging scenario (**Table 4**). For $n = 6$ and high noise ($\sigma = 5$), coverage of x^* dropped to 61% and bias increased to 2.1 units, a consequence of the difficulty in accurately estimating the phase of the cosine curves with very few points. However, for $n \geq 10$ and $\sigma \leq 2$, coverage recovered to 84–93% and bias was substantially reduced. Coverage of y^* remained consistently high ($\geq 93\%$) across all scenarios. Given these limitations, we treat the cosine model as exploratory in the present applications; further validation would be valuable before its use in confirmatory settings.

Table 2. Performance of the DIAS for the linear model.

n	σ	Bias(x)	RMSE(x)	Cov(x) (%)	Bias(y)	RMSE(y)	Cov(y) (%)	Conv. (%)
6	1	−0.009	0.296	91.3	0.003	0.281	95.9	100
6	2	−0.001	0.626	90.7	0.004	0.593	95.4	100
6	5	−0.105	2.792	96.2	−0.076	2.039	95.5	100
10	1	0.004	0.231	92.6	0.007	0.216	97.6	100
10	2	−0.003	0.452	94.6	−0.023	0.467	97.1	100
10	5	−0.059	3.941	97.1	−0.107	1.787	97.6	100
20	1	−0.003	0.162	93.4	0.005	0.152	98.9	100
20	2	−0.002	0.326	93.7	0.003	0.320	99.1	100
20	5	−0.019	0.917	96.8	0.026	0.817	99.3	100

Table 3. Performance of the DIAS for the 3-parameter sigmoid model.

n	σ	Bias(x)	RMSE(x)	Cov(x) (%)	Bias(y)	RMSE(y)	Cov(y) (%)	Conv. (%)
6	1	0.001	0.028	89.9	0.034	0.817	82.4	99.6
6	2	−0.002	0.055	91.1	0.039	1.550	82.9	99.4
6	5	0.020	0.221	91.2	0.902	5.618	78.0	99.9

10	1	0.000	0.021	91.4	0.033	0.600	87.0	99.3
10	2	−0.003	0.043	92.2	−0.032	1.202	86.9	99.4
10	5	−0.005	0.110	94.0	0.100	3.149	86.1	99.8
20	1	0.001	0.015	94.3	0.028	0.407	90.3	99.5
20	2	0.001	0.027	96.1	0.060	0.803	89.6	99.8
20	5	0.002	0.075	95.4	0.165	2.150	87.8	99.9

Table 4. Performance of the DIAS for the cosine model (first intersection).

n	***σ***	**Bias(*x*)**	**RMSE(*x*)**	**Cov(*x*) (%)**	**Bias(*y*)**	**RMSE(*y*)**	**Cov(*y*) (%)**	**Conv. (%)**
6	1	0.456	1.184	85.2	0.026	0.460	93.5	100
6	2	1.191	1.940	69.7	−0.009	0.984	92.8	95.0
6	5	2.115	2.836	60.9	−0.132	2.496	93.3	81.0
10	1	0.282	0.942	90.2	0.014	0.375	96.2	100
10	2	0.950	1.706	76.0	0.039	0.740	97.0	97.3
10	5	2.023	2.650	54.7	−0.010	2.003	97.5	83.9
20	1	0.132	0.629	93.3	0.016	0.267	98.7	100
20	2	0.626	1.386	84.0	0.027	0.531	98.6	99.6
20	5	1.582	2.262	61.5	−0.014	1.379	98.9	88.5

3.3. Summary of simulation findings

The Monte Carlo study demonstrates that the DIAS estimator is approximately unbiased and that the standard errors obtained via the Delta Method yield confidence intervals with adequate coverage for moderate sample sizes ($n \geq 10$) and typical noise levels. The linear model performed well; the sigmoid model showed slightly reduced coverage for y* due to the inherent nonlinearity; the cosine model, although more sensitive to small samples and high noise, performed adequately for $n \geq 10$. These results support using the DIAS to estimate the intersection point in coupled curve problems.

3.4. Parametric bootstrap validation

To evaluate the comparison procedure, we tested a parametric bootstrap for type I error and power under the linear and 3-parameter sigmoid models. Under the null hypothesis, the bootstrap rejection rates remained close to the nominal 5% in all

scenarios (linear: 3.6%-5.4%; sigmoid: 2.3%-5.1%). Power was high for moderate to strong effects under low noise (σ = 1), reaching 83%-100% for the linear model and 89%-100% for the sigmoid model with n = 6-20. Under high noise (σ = 5), power decreased for small effects, as expected, but remained adequate for strong effects and larger samples. These results support the use of the bootstrap p-value as a calibrated alternative to the Wald test, particularly for small samples and nonlinear models. Detailed tables are provided in the Supplementary Material.

4. APPLICATIONS

4.1. DIAS confirm the relationship between NO and H_2O_2 pathways in endothelium-dependent relaxation

We reanalysed data from Capettini et al. (2010) [1], focusing on the effect of eNOS AS-ODN on the relationship between H_2O_2 production and relaxation. The DIAS was computed as the intersection point between the mediator production curve and the relaxation curve, with error propagation via the Delta Method.

In the AS-ODN experiment (**Figure 1A**), the control group DIAS was DIAS-X = −7.156 ± 0.064 (Log[ACh]) and DIAS-Y = 72.5 ± 1.86 (%). After AS-ODN treatment, the DIAS shifted to DIAS-X = −6.377 ± 0.068 (Log[ACh]) and DIAS-Y = 31.8 ± 2.52 (%). The parametric bootstrap test indicated a significant difference ($p < 0.001$). The bivariate Wald statistic was W = 395.856 (D^2 = 19.896).

The DIAS reanalysis is consistent with the functional contribution of the NO pathway to ACh-dependent relaxation, as originally demonstrated by Capettini et al. (2010) [1]. The large difference in DIAS between control and treated groups quantifies the impact of inhibiting eNOS on the coupling between mediator production and vascular response. The DIAS thus provides an integrative metric that complements traditional EC50 and E_{max} analyses by offering a direct measure of signalling pathway efficiency.

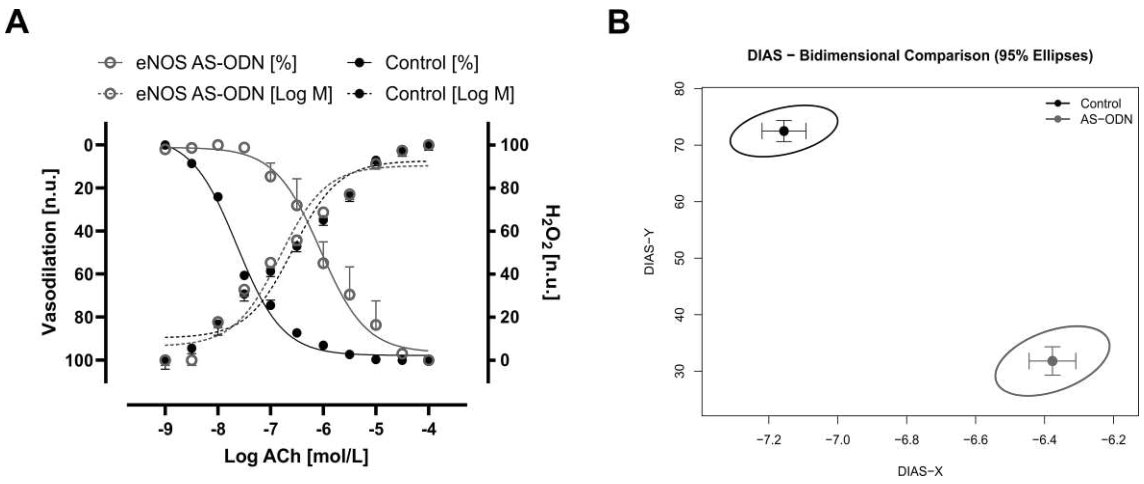


Figure 1. Reanalysis of the data from Capetinni et al. (2010) regarding the effect of AS-ODN. **(A)** Normalized data originally extracted from Fig. 4B of the original reference. **(B)** Ellipses comparing the DIAS of the coupled control and AS-ODN curves.

4.2. DIAS reveals differential blockade of dopamine by eticlopride at D_2 and α_2A receptors

Reanalysis of data from Figure 6B of Avet et al. (2022) [18] using the DIAS revealed substantial differences in eticlopride-mediated dopamine blockade, both in potency (DIAS-X; Log[DA]) and residual response (DIAS-Y; %).

At the D_2 receptor, the DIAS for $G\alpha i_2$ was DIAS-X = −8.994 ± 0.066 (Log[DA]) and DIAS-Y = 20.3 ± 2.52 (%), whereas for GαoB it was DIAS-X = −9.475 ± 0.025 (Log[DA]) and DIAS-Y = 55.10 ± 1.68 (%). The difference in DIAS-X was 0.481 log units, indicating greater potency of blockade at GαoB. The most striking difference, however, was in DIAS-Y: a 34.8 percentage-point gap, showing that at GαoB the residual response is substantially larger, suggesting less effective blockade. The parametric bootstrap test indicated a significant difference ($p < 0.001$). The bivariate Wald statistic was $W = 141.524$ ($D^2 = 11.896$).

At the α_2A receptor (coupled to $G\alpha i_2$), the DIAS was DIAS-X = −6.629 ± 0.031 (Log[DA]) and DIAS-Y = 30.70 ± 1.52 (%). Comparison with $D_2/G\alpha i_2$ revealed a difference of 2.365 log units in DIAS-X, indicating high selectivity of eticlopride for D_2 over α_2A. The difference in DIAS-Y was 10.4 percentage points, smaller than the between-pathway difference observed at D_2. The parametric bootstrap test indicated

a significant difference ($p < 0.001$). The bivariate Wald statistic was $W = 1391.413$ ($D^2 = 37.302$).

The application of the DIAS to the data of Avet et al. (2022) [18] demonstrates that eticlopride is not a uniform antagonist (**Figure 2A and 2C**). The bivariate analysis indicated that selectivity between receptors (D_2 vs. α_2A) is predominantly a matter of potency (DIAS-X), whereas signalling bias between pathways at D_2 ($G\alpha i_2$ vs. $G\alpha oB$) involves both potency and, more markedly, the residual response (DIAS-Y). These findings highlight the value of the DIAS as a tool that goes beyond EC50, capturing the multidimensional complexity of antagonist pharmacology.

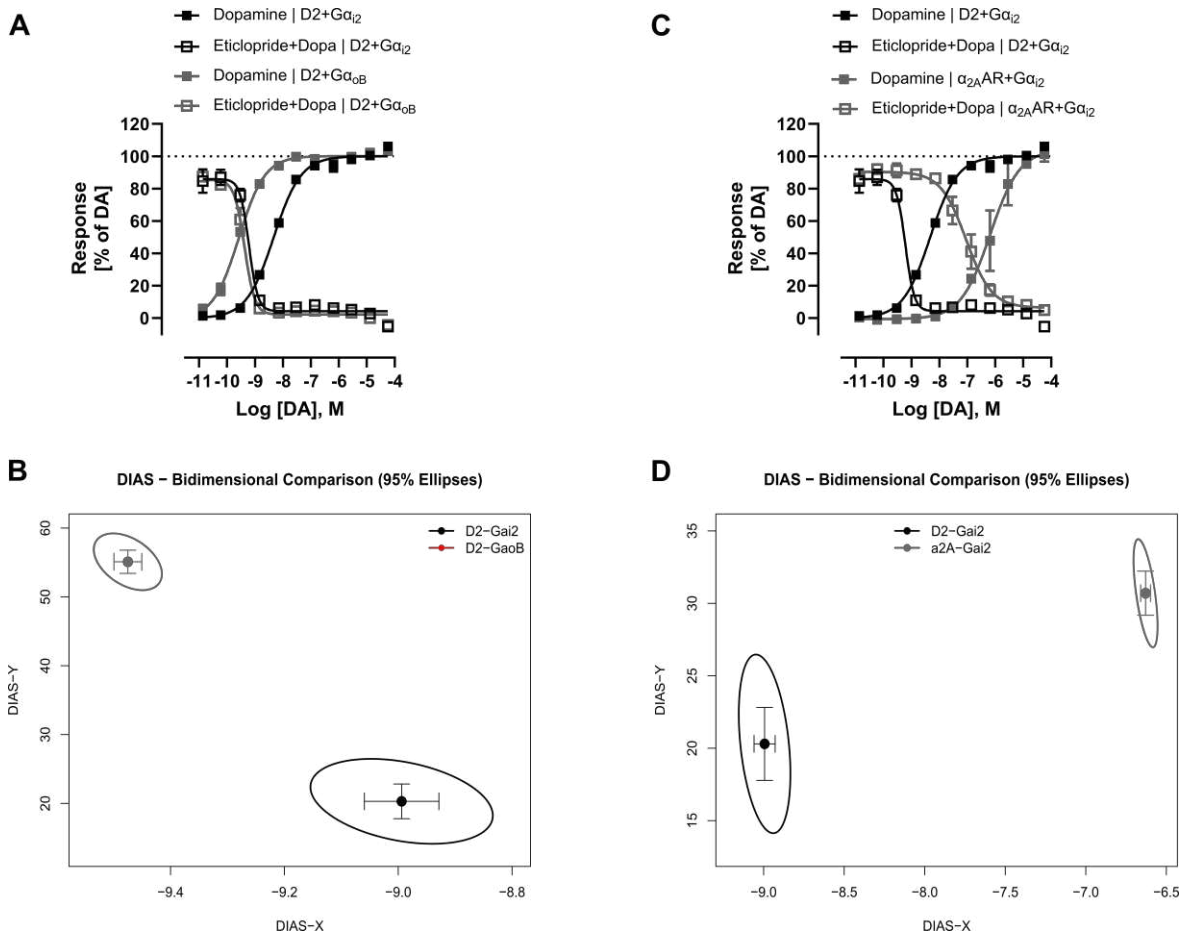


Figure 2. Reanalysis of the data from Avet et al. (2022) concerning the dynamics of dopamine and its D_2 and α_2A receptors. **(A)** Extracted data from Fig. 6B of the original reference. **(B)** Ellipses comparing the DIAS of the coupled D_2-$G\alpha i_2$ versus D_2-$G\alpha oB$. **(C)** Extracted data from Fig. 6B of the original reference. **(D)** Ellipses comparing the DIAS of the coupled D_2-$G\alpha i_2$ versus α_2A-$G\alpha i_2$.

4.3. DIAS quantifies the predator-prey equilibrium point in normalized capelin-cod dynamics

To illustrate the applicability of the DIAS as a descriptive metric in coupled systems, we reanalysed data from Figure 5C of Pednekar et al. (2024) [2]. This figure presents two curves describing the interaction between cod (predator) and capelin (prey): cumulative capelin consumption (Curve 1) and capelin survival (Curve 2), both as functions of time (**Figure 3A**). Although the original authors did not fit a regression to the data, the visual distribution of points suggests a robust linear relationship for both variables, justifying the use of the linear model for DIAS computation.

Because the two variables are measured on different scales (cumulative consumption in number of individuals, survival in percentage), min-max normalisation to 0-100% was applied to both curves, enabling direct comparison and the calculation of a biologically meaningful intersection point. The resulting DIAS therefore refers to the equilibrium point on the normalised scale (**Figure 3B**).

The linear fits to the normalised data yielded the following parameters: Curve 1 (normalised cumulative consumption): intercept = 4.32 ± 0.52, slope = 0.4124 ± 0.0038, adjusted R^2 = 0.99; Curve 2 (normalised survival): intercept = 88.29 ± 1.28, slope = −0.3986 ± 0.0093, adjusted R^2 = 0.97. The DIAS was calculated as DIAS-X = 103.524 ± 0.892 (minutes) and DIAS-Y = 47.0 ± 0.27 (normalised units). This intersection point represents the moment at which cumulative consumption and survival are equal in relative terms, i.e., the dynamic equilibrium between predation and survival. Although not numerically identical to the visual crossing in the original graph (due to normalisation), it provides a standardised, comparable metric to describe the ecological balance.

The DIAS thus provides a quantitative estimate, with standard error, of the equilibrium point between two coupled variables, even when they are originally expressed on different scales, provided they are normalised to a common scale. The high adjusted R^2 values of the linear fits (0.99 and 0.97) indicate excellent model adequacy and, consequently, high reliability of the estimated intersection point. This example opens avenues for future applications in which DIAS values from different

experimental conditions could be statistically compared using the bootstrap procedure described in Section 2.3.

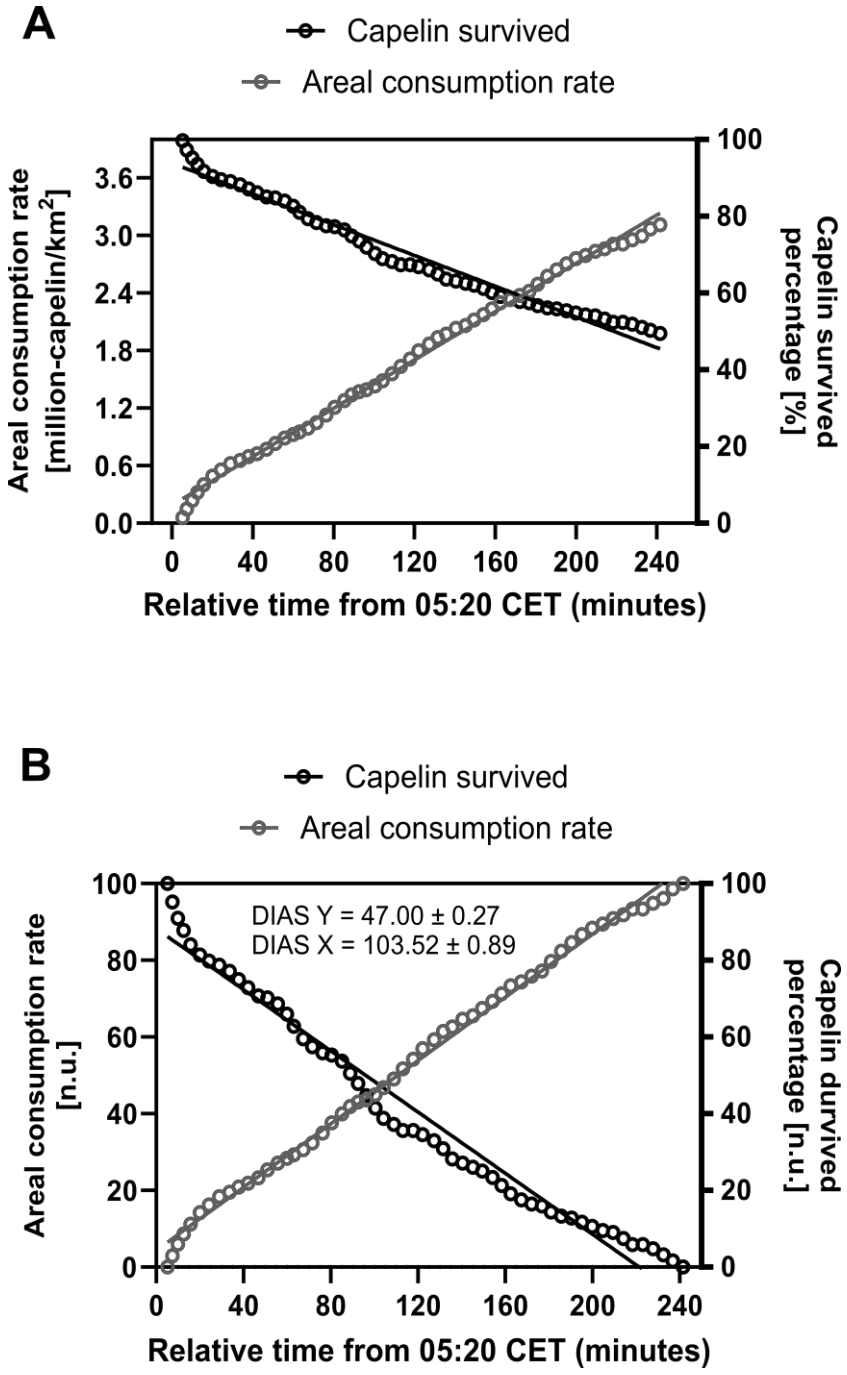


Figure 3. Reanalysis of the data from Pednekar et al. (2024) on the predator-prey relationship. **(A)** Extracted data from Fig. 5C of the original reference. **(B)** The same results as in A, with normalized units.

4.4. DIAS identifies asynchronous urban transitions in Brazilian states

To demonstrate the applicability of the DIAS to demographic data, we analysed the urbanisation trajectories of two Brazilian states, Minas Gerais (MG) and Rio Grande do Sul (RS), using census data from 1950 to 2010 (IBGE, Brazilian Institute of Geography and Statistics). The percentage of urban and rural populations in each state was treated as coupled curves (% urban + % rural = 100%), and the DIAS was computed as the year in which the two curves intersect - i.e., the moment when the population became predominantly urban (**Figure 4A**).

Linear regression provided excellent fits for all curves ($R^2 > 0.98$). For MG, the urban and rural curves intersected at DIAS-X = 1968.07 ± 1.31 years and DIAS-Y = 50.0 ± 1.80%. For RS, the intersection occurred at DIAS-X = 1973.75 ± 1.03 years and DIAS-Y = 50.0 ± 1.29%. Both states reached the 50% urban threshold in the late 1960s to mid-1970s, but MG completed the transition approximately 5.7 years earlier than RS. The parametric bootstrap test indicated a significant difference ($p = 0.011$). The bivariate Wald statistic was $W = 23.210$ ($D^2 = 4.820$). The confidence ellipses for the two states are well separated (**Figure 4B**), visually reinforcing the conclusion that the urbanisation processes were asynchronous.

This example illustrates three important features of the DIAS. First, even when the DIAS-Y is constrained by definition (here, % urban = % rural = 50%), the uncertainty in DIAS-X can be substantial and informative. Second, the DIAS is capable of detecting significant temporal differences between regions with very similar overall trajectories, which is a distinction that would be difficult to quantify with descriptive statistics alone. Third, the method handles complementary curves naturally, without requiring any special treatment.

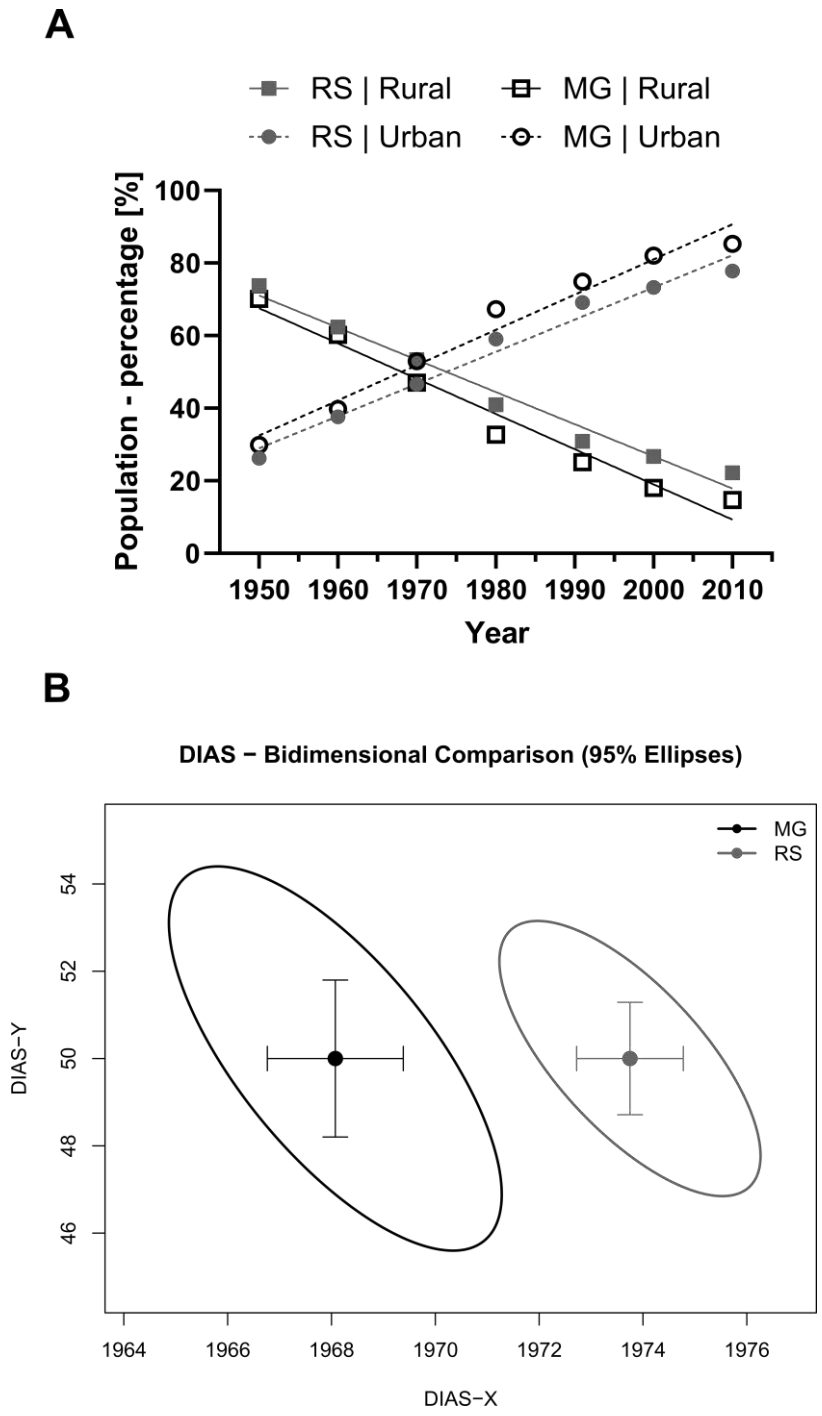


Figure 4. **(A)** Linear relationship between the urbanization process in RS and MG. Original data sourced from the IBGE. **(B)** Ellipses illustrating a comparison of the coupled relationship in RS and MG.

4.5. DIAS detects stable thermal equilibrium points between two Brazilian cities across decades

To showcase the DIAS in a periodic system with multiple intersections, we analysed mean monthly temperatures of two Brazilian cities with contrasting climates: Brasília (tropical savanna) and Porto Alegre (subtropical). Data were obtained from the Brazilian National Institute of Meteorology (INMET) for two 30-year climatological normal periods: 1961-1990 and 1991-2020. For each period, a cosine model with a fixed 12-month period was fitted to the monthly temperatures, yielding two annual intersections: one in autumn (March-April) and one in spring (September-October).

1961-1990 period. The cosine model fit well (Brasília: $R^2 = 0.95$; Porto Alegre: $R^2 = 0.99$). Two DIAS were identified: DIAS 1 at $X = 3.63 \pm 0.25$ months (mid-March), $Y = 21.0 \pm 0.16$°C; and DIAS 2 at $X = 10.19 \pm 0.26$ months (early October), $Y = 21.4 \pm 0.17$°C.

1991-2020 period. The model again fitted well (Brasília: $R^2 = 0.96$; Porto Alegre: $R^2 = 0.99$). The two DIAS were: DIAS 1 at $X = 3.69 \pm 0.28$ months, $Y = 21.8 \pm 0.19$°C; and DIAS 2 at $X = 10.50 \pm 0.28$ months, $Y = 22.2 \pm 0.19$°C.

Comparison between periods. We applied bivariate Wald tests to each pair of corresponding DIAS points separately, adjusting p-values with a Bonferroni correction for two comparisons. Neither the autumn intersection (DIAS 1: 1961-90 vs. 1991-2020; $W = 0.05$, adjusted $p = 1.000$) nor the spring intersection (DIAS 2: 1961-90 vs. 1991-2020; $W = 0.12$, adjusted $p = 1.000$) showed a significant shift between periods. The parametric bootstrap procedure yielded p-values greater than 0.05 for both comparisons, consistent with the Wald results. These results indicate that the thermal equilibrium points between Brasília and Porto Alegre have remained remarkably stable over six decades (**Figure 5**).

Within each period, the two annual intersections (DIAS 1 vs. DIAS 2) remain highly distinct (1961-90: $W = 177.9$, $p < 0.001$; 1991-2020: $W = 157.2$, $p < 0.001$), indicating that autumn and spring represent significantly different thermal meeting points.

The DIAS analysis reveals that although the mean temperatures at the intersection points have risen by approximately 0.8°C (consistent with global warming trends); the months when the two cities' temperatures equalise have not changed (**Figure 5**). This suggests a proportional warming across seasons in both cities, that is, the seasonal temperature curves have shifted upward in parallel, preserving the timing of their crossings. This finding illustrates the DIAS' ability to decompose complex spatiotemporal questions into testable hypotheses about both the value (DIAS-Y) and the timing (DIAS-X) of coupled-curve intersections.

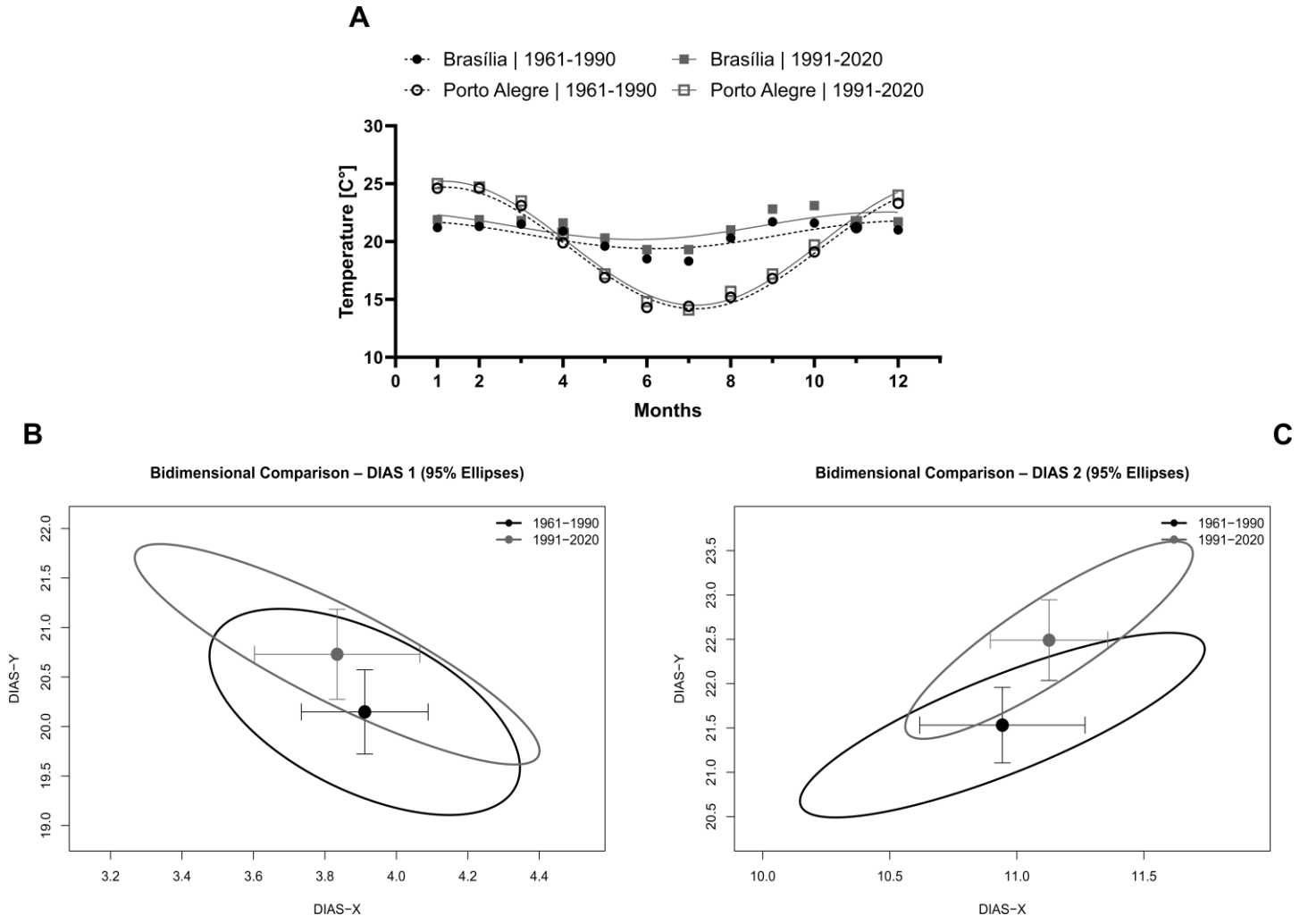


Figure 5. **(A)** Average monthly temperatures in Brasília and Porto Alegre during different periods. Original data sourced from INMET. **(B)** Comparison of the first pair of DIAS found: overlapping ellipses indicate no difference. **(C)** Comparison of the second pair of DIAS found: overlapping ellipses indicate no difference.

5. DISCUSSION

5.1. Generality of the DIAS

The results presented in the previous sections demonstrate that the DIAS is a flexible metric, applicable to different curve types (linear, sigmoid, cosine) and to problems originating from distinct knowledge domains (pharmacology, ecology, demography, climatology). This generality stems from the fact that the DIAS does not depend on the functional form of the curves, but only on the existence of an intersection point that can be computed numerically and on parameter estimates with their covariance matrices. The DIAS is best understood as a practical addition to the existing toolkit for curve analysis, rather than a replacement for well-established methods.

Our review revealed that, although numerous methods exist for comparing curves (global tests [5, 8], pointwise comparisons [6, 7], and equivalence tests [10]), none of them estimates the intersection point with error propagation and a bivariate hypothesis test. The DIAS, therefore, does not compete with these methods but complements them, offering a tool for a problem that previously lacked a formal statistical treatment.

5.2. Interpretation of the Wald test, bootstrap, and confidence ellipses

A point that deserves attention is the relationship between the bivariate Wald test, the parametric bootstrap, and the visual inspection of the 95% confidence ellipses. The ellipses represent individual confidence regions for each DIAS. Partial overlap of two ellipses does not necessarily imply the absence of a difference. Non-overlapping ellipses almost always indicate a clear difference. The ellipses should be interpreted as a visual aid rather than as a formal test.

The bivariate Wald test provides a fast approximation, but our simulations showed that it can be liberal for small samples and nonlinear models. We therefore regard the Wald p-value as exploratory. For confirmatory conclusions, we used and recommend the parametric bootstrap p-value, which better controlled the type I error in our simulations. This distinction, although subtle, is analogous to the difference between comparing individual confidence intervals and performing a calibrated hypothesis test on the difference between two parameters [19].

5.3. Choice of the search interval for the intersection

In the computational implementation of the DIAS, determining the intersection point x^* requires, for nonlinear models, the specification of a search interval. For sigmoidal curves, the interval is automatically centred around the estimated LogEC50; for cosine curves, the interval spans one full period defined by the user. Although this choice is a computational artefact rather than a theoretical limitation of the method, the interval must contain the true intersection. In all applications and simulations presented here, visual inspection confirmed the adequacy of the intervals used. In ambiguous situations (e.g., curves with multiple very close crossings), it is recommended that the user graphically examine the data before defining the interval. The inclusion of an automatic procedure for detecting the number of intersections is a possible future extension of the method.

5.4. Independence between curves and the block-diagonal structure

The computation of the DIAS covariance matrix via the Delta Method assumes that the two coupled curves are fitted to independent data, resulting in a block-diagonal joint covariance matrix. This assumption is reasonable in most applications, for example, when the curves originate from distinct experimental assays or from variables measured in different units. However, in situations where the two curves share the same source of variability (e.g., two responses measured on the same individuals), the independence assumption may be violated. In such cases, the joint covariance matrix should include the cross-covariance terms between the parameters of the two curves. Extending the DIAS to paired data, with appropriate estimation of the cross-covariance, constitutes a promising direction for future work.

Conversely, when the two curves are complementary by construction (as in the demographic example, where % urban + % rural = 100%), the residuals of one curve are the exact negative of the residuals of the other. Under this exact complementarity, a negative cross-covariance between the estimated parameters is expected, although it was not explicitly modelled in the present analysis. The block-diagonal structure adopted here therefore treats the two curves as independent, which is a simplification. While this assumption is not expected to invalidate the conclusions reported in

Section 4.4, a formal evaluation of its impact under non-zero cross-covariance represents an avenue for future work.

5.5. Validation of the Monte Carlo simulations and limitations

The Monte Carlo simulations demonstrated that the DIAS estimator is approximately unbiased and that the confidence intervals based on the Delta Method achieve coverage close to the nominal level (95%) for moderate sample sizes ($n \geq 10$) in the linear and sigmoid models. For the cosine model, the coverage of the X-axis proved sensitive to small samples ($n = 6$) with high noise ($\sigma = 5$), reaching only 61%. This behaviour does not represent a failure of the DIAS but reflects the intrinsic difficulty of estimating the phase of periodic curves with few points, which is a challenge well documented in the analysis of circadian rhythms [3]. For applications with $n \geq 10$ and noise levels typical of experimental data ($\sigma \leq 2$), the performance of the DIAS was satisfactory (coverage ≥ 84%).

The parametric bootstrap comparison was also evaluated for the linear and 3-parameter sigmoid models. Under the null hypothesis, the bootstrap rejection rates remained close to the nominal 5% in all scenarios (linear: 3.6%-5.4%; sigmoid: 2.3%-5.1%). Power was high for moderate to strong effects under low noise, reaching 83%-100% for the linear model and 89%-100% for the sigmoid model with $n = 6$ to 2020. Under high noise, power decreased for small effects, as expected, but remained adequate for strong effects and larger samples. These results support the use of the bootstrap p-value as a calibrated alternative to the Wald test.

Importantly, the DIAS does not assume that an intersection exists or that it is unique. The intersection is found numerically within a user-defined search interval. When multiple intersections exist (e.g., periodic curves), the method applies separate comparisons to each pair of corresponding DIAS points with a multiplicity adjustment. It is important to note that the current simulations validated the individual DIAS estimator. A multivariate Wald test that jointly compares multiple intersections was initially considered but proved to be excessively liberal in our investigations. We therefore do not recommend its use for confirmatory inference. Instead, separate bootstrap comparisons with a multiplicity adjustment are preferred when multiple intersections are present.

5.6. Future applications

Beyond the examples presented here, the DIAS holds promise for a variety of other domains. In chronobiology and circadian physiology, for instance, researchers often compare the temporal expression profiles of two clock genes (e.g., *Per2* vs. *Bmal1*) measured in the same tissue over a 24-hour cycle. Current methods, such as CircaCompare [4], test for differences in individual cosine parameters (mesor, amplitude, phase) between two rhythms but do not estimate the time points at which the expression levels of the two genes are equal. The DIAS, with its cosine model and the ability to compare multiple intersections via separate bootstrap tests with multiplicity adjustment, could provide a direct answer to questions such as: "At what circadian times do the expression profiles of *Per2* and *Bmal1* intersect, and does this intersection shift under a clock gene knockout?" In renal physiology, the coupled relationship between antidiuretic hormone, urine osmolarity, and urinary flow rate represents another scenario in which the DIAS could quantify the point at which two physiological processes (concentration and dilution) are balanced. Similarly, in calcium metabolism, the opposing effects of parathyroid hormone and calcitonin on plasma Ca^{2+} concentration could be analysed by identifying the intersection point of their dose–response curves, providing a quantitative measure of their relative activities.

The applicability of the DIAS extends well beyond the biomedical sciences. In ecology, for example, growth curves of competing species could be compared to determine the time at which one species becomes numerically dominant. In economics, the intersection of supply and demand curves defines the market equilibrium price; the DIAS could be used to compare equilibrium points across regions or time periods. In materials science and engineering, stress-strain curves of different materials could be analysed to identify the deformation level at which their mechanical responses become equivalent. These examples illustrate that the DIAS is not restricted to biological systems but provides a general inferential framework for any domain in which coupled curves meet. The development of domain-specific implementations, such as an R package tailored for circadian data, would further facilitate adoption.

5.7. Limitations and future directions

In addition to the limitations already discussed, the DIAS presents others that deserve consideration. First, in several applications presented here (notably the predator–prey equilibrium and the NO-dependent relaxation experiment), the two coupled curves were originally expressed on different scales (e.g., cumulative consumption in number of individuals vs. survival in percentage; NO production in arbitrary units vs. relaxation as % of maximum). In such cases, a normalisation step (e.g., min-max scaling to 0-100%) was necessary to bring the curves onto a common scale before computing the DIAS. Normalisation alters the numerical value of the DIAS-Y and may shift the DIAS-X; therefore, the resulting DIAS refers to the equilibrium point on the normalised scale, not on the original measurement scale. When both curves are expressed in the same natural units, the DIAS can be interpreted as an intrinsic property of the data. When normalisation is required, the scaling procedure should be explicitly reported, and sensitivity of the results to alternative normalisations should be considered. In the present applications, the same normalisation was applied to all groups, allowing valid within-study comparisons, but the absolute value of the DIAS should not be compared across studies that used different scaling procedures. A sensitivity analysis exploring the effect of alternative normalisation strategies is provided in the Supplementary Material.

It should be noted that min–max normalisation, while deterministic, uses sample-dependent quantities (minimum and maximum) that are themselves subject to sampling variability. In the present applications, the high R^2 values of the fitted curves (all > 0.97) suggest that the normalisation step introduces negligible additional uncertainty. For small samples or when the extremes are poorly estimated, this additional source of uncertainty may become non-negligible and is explored in the Supplementary Material.

Second, the method depends on the convergence of the curve-fitting algorithm (e.g., nonlinear least squares). In scenarios with very noisy data or poorly specified models, parameter estimation may fail, making the computation of the DIAS impossible. The convergence rates observed in the simulations were above 99% for the linear and sigmoid models, but dropped to 81% in the most extreme cosine scenario. Third, the Delta Method provides an asymptotic approximation that may be imprecise for very

small samples. Although the simulations showed adequate coverage for $n \geq 10$, applications with $n \leq 6$ should be interpreted with caution. Fourth, the parametric bootstrap, while better calibrated than the Wald test, is computationally more expensive and may not be practical for very large datasets or extensive simulation studies. Its use is recommended for confirmatory inference, whereas the Wald test may be retained for initial exploration.

Promising directions for extending the DIAS include: (i) the development of a Bayesian implementation of the DIAS, which would complement the Delta Method by providing exact finite-sample inference and allowing the incorporation of prior information when available; (ii) the extension to paired data, with estimation of the cross-covariance between the curves; (iii) the implementation of an automatic procedure for detecting the number of intersections; (iv) the release of an R package on CRAN, complementing the existing Shiny application; and (v) the application of the DIAS to other curve types, such as exponential decay or polynomial models, expanding its reach to new fields.

5.8. Practical implications, recommendations, and software availability

Although the DIAS Shiny application performs curve fitting internally, we strongly recommend that users first fit the chosen model (linear, sigmoid, cosine, etc.) in their preferred statistical software and visually inspect the fitted curves, residuals, and goodness-of-fit metrics. This preliminary step helps identify poor fits, outliers, or violations of model assumptions that could compromise the DIAS estimate. In particular, for the linear model, verifying linearity and homoscedasticity is straightforward and can prevent meaningless results when the true relationship is nonlinear. The DIAS app provides residual plots and R^2 values to assist this evaluation, but the final decision on model adequacy rests with the investigator.

The DIAS Shiny application, freely available at [https://r-dias.shinyapps.io/DIAS/], implements all the methods described in this paper. It allows researchers without programming experience to perform complete curve-intersection analyses, from model fitting to Wald tests, parametric bootstrap p-values, and ellipse plots. The source code of the application and the simulation scripts are provided as

Supplementary Material, ensuring full reproducibility of the results presented. Users are encouraged to report bugs or suggest improvements via the contact information provided in the app.

6. CONCLUSION

The DIAS provides a simple, statistically rigorous answer to a question that arises across many scientific domains: where do two coupled curves intersect, and does that intersection change between conditions? The method performed adequately in Monte Carlo simulations and was applicable across five diverse applications that went from pharmacology to ecology, demography, and climatology. The DIAS does not replace existing tools for curve comparison; it complements them by offering a formal method for estimating and comparing the intersection point of two coupled curves, with uncertainty propagation and a calibrated bootstrap comparison procedure. A free, open-source Shiny application makes the method immediately accessible to the research community.

7. DATA AVAILABILITY STATEMENT

The data used in this work were extracted from published articles and public sources: Capettini et al. (2010) [1], Avet et al. (2022) [18], Pednekar et al. (2024) [2], IBGE, and INMET. The code for the Shiny application is available at [https://r-dias.shinyapps.io/DIAS/]. Scripts for simulations are provided as Supplementary Material.

8. ACKNOWLEDGMENTS

The author thanks Professor Renan Pedra de Souza (UFMG/Fiocruz Minas) for his careful reading of an earlier version of this manuscript. His insightful comments, constructive criticism, and encouragement not only improved the clarity and rigour of the work but also strengthened the confidence in the contribution it offers. The author would like to thank Professor Virgínia Soares Lemos (UFMG/ICB) for her trust and encouragement; it is a privilege to count on colleagues whose dedication and scientific generosity make the process of research more human and more precise.

This work was funded by: “Coordenação de Aperfeiçoamento de Pessoal de Nível Superior (CAPES) Edital PDPG III - Parcerias Estratégicas com os estados III; Fundação de Amparo à Pesquisa do Estado de Minas Gerais (FAPEMIG) APQ-04900-22”.
The author used AI-based tools for language and image editing. All content was reviewed and approved by the author.

The datasets and scripts supporting this study, as well as the supplementary materials, are available from the corresponding author upon reasonable request and will be made publicly available upon publication.

The author declares no conflict of interest.

9. REFERENCES

1. Capettini, L.S., V.S. Cortes Sf Fau - Lemos, and V.S. Lemos, Relative contribution of eNOS and nNOS to endothelium-dependent vasodilation in the mouse aorta. 2010(1879-0712 (Electronic)).
2. Pednekar, S., et al., Rapid predator-prey balance shift follows critical-population-density transmission between cod (Gadus morhua) and capelin (Mallotus villosus). Communications Biology, 2024. 7(1): p. 1386.
3. Refinetti, R., G. Cornélissen, and F. Halberg, Procedures for numerical analysis of circadian rhythms. Biological Rhythm Research, 2007. 38(4): p. 275-325.
4. Parsons, R., et al., CircaCompare: a method to estimate and statistically support differences in mesor, amplitude and phase, between circadian rhythms. Bioinformatics, 2020. 36(4): p. 1208-1212.
5. Li, H., et al., Statistical inference methods for two crossing survival curves: a comparison of methods. PLoS One, 2015(1932-6203 (Electronic)).
6. Herberich, E., C. Hassler, and T. Hothorn, Multiple Curve Comparisons with an Application to the Formation of the Dorsal Funiculus of Mutant Mice. 2014. 10(2): p. 289-302.
7. Oleson, J.J., et al., Detecting time-specific differences between temporal nonlinear curves: Analyzing data from the visual world paradigm. Statistical Methods in Medical Research, 2017. 26(6): p. 2708-2725.
8. Hristova, K. and W.A.-O. Wimley, Determining the statistical significance of the difference between arbitrary curves: A spreadsheet method. 2023(1932-6203 (Electronic)).
9. Rocchetti, M. and G. De Nicolao, CURT: a randomization test for statistical comparison between experimental curves. Computer Methods and Programs in Biomedicine, 1990. 31(3): p. 207-213.
10. Dette, H., et al., Equivalence of Regression Curves. Journal of the American Statistical Association, 2018. 113(522): p. 711-729.
11. Oehlert, G.W., A Note on the Delta Method. The American Statistician, 1992. 46(1): p. 27-29.

12. Beutner, E., Delta method, asymptotic distribution. WIREs Computational Statistics, 2024. 16(1): p. e1634.
13. Phillips, P.C.B., The Exact Distribution of the Wald Statistic. Econometrica, 1986. 54(4): p. 881-895.
14. Bernard, D.R., Multivariate Analysis as a Means of Comparing Growth in Fish. Canadian Journal of Fisheries and Aquatic Sciences, 1981. 38(2): p. 233-236.
15. Zhang, J.-T., et al., A Simple Two-Sample Test in High Dimensions Based on L2-Norm. Journal of the American Statistical Association, 2020. 115(530): p. 1011-1027.
16. Haoran, L., et al., An adaptable generalization of Hotelling's T2 test in high dimension. The Annals of Statistics, 2020. 48(3): p. 1815-1847.
17. Eckert, M. and W. Vach, Visualizing uncertainty in a two-dimensional estimate using confidence and comparison regions. The Stata Journal, 2023. 23(2): p. 455-490.
18. Avet, C., et al., Effector membrane translocation biosensors reveal G protein and βarrestin coupling profiles of 100 therapeutically relevant GPCRs. 2022(2050-084X (Electronic)).
19. Schenker, N. and J.F. Gentleman, On Judging the Significance of Differences by Examining the Overlap Between Confidence Intervals. The American Statistician, 2001. 55(3): p. 182-186.

Supplementary Files

This is a list of supplementary files associated with this preprint. Click to download.

- SupplementarysubmissionRS.docx
- estimatorvalidation.r
- sensitivityh.r
- sensitivitynormalisation.r
- bootstrapvalidation.r
- DIASapp.r